inter-noise 2002

The 2002 International Congress and Exposition on Noise Control Engineering
Dearborn, MI, USA. August 19-21, 2002

Effect of Rotation on the Vibration Characteristics of Tires

Yong-Joe Kim and J. Stuart Bolton
1077 Ray W. Herrick Laboratories, School of Mechanical Engineering, Purdue University
West Lafayette, Indiana 47907-1077, USA

Abstract

It was shown previously that a wave number decomposition of the radial vibration measured on the surface of a static tire reveals the dispersion characteristics of the waves that contribute to the tire's dynamic response. In addition it was found that a circular cylindrical shell model of the tire treadband with air pressure acting on its interior surface successfully reproduced the main characteristics of the experimental dispersion relations. To identify the wave propagation effects of tire rotation, rotation of the shell about a fixed axis that simulates the axle of a car has been considered here. The equations of motion of a rotating circular cylindrical shell were derived in a fixed reference frame. From those equations, the analytical dispersion relation was obtained after assuming propagating solutions for the free vibration case. The forced solution can be then calculated when the system is driven by a point force at a fixed location in the reference frame. The latter results were interpreted physically in terms of wave propagation in the rotating system from the viewpoint of a fixed observer. The dispersion relations of a rotating tire were also compared with those of the static tire. It was shown that at typical rotational speeds, a static tire analysis could be used to predict the characteristics of the rotating tire after a simple kinematic compensation was performed.

1. Introduction

Two earlier articles [1,2] dealt with static tire dispersion relations that characterize both tire dynamics and their potential for sound radiation. The first article described both an experimental measurement procedure and a wave number decomposition technique for analyzing the measured data. The second article described simple analytical and numerical models of tire treadbands that were found to reproduce the significant features of measured tire dispersion relations. The objective here was to extend the previous analytical model [2] to determine how a tire's rotation affects its dispersion relations. For this purpose, the tire treadband has been modeled as a simply

supported, rotating circular cylindrical shell having finite width. Both inflation pressure and rotational stiffening were accounted for in this model.

Equations of motion and solutions for the case of rotating circular cylindrical shell were previously obtained by Huang and Soedel [3]. Those equations and solutions were formulated in a local coordinate system that was assumed to rotate with the shell. That type of formulation makes it difficult to apply a sinusoidal point force at a fixed point simulating a contact patch excitation of a rotating tire, since the response is Doppler shifted in the local frame in that case. In contrast, a system described in fixed, or reference, coordinates, as here, responds at the frequency of the input force. Huang and Soedel also expressed their results in terms of mode shapes: here a wave approach has been followed. Finally, the $n = 0$ circumferential mode, which can be very important in terms of sound radiation, was not considered in their work. Another approach was followed by Vinesse and Nicollet [4], who modeled a tire as a two-dimensional membrane in reference coordinates. They obtained dispersion relations from a natural vibration analysis and obtained the forced response to a rotating point force using a wave solution. In their work, however, effects of flexural stiffness and circumferential curvature were neglected.

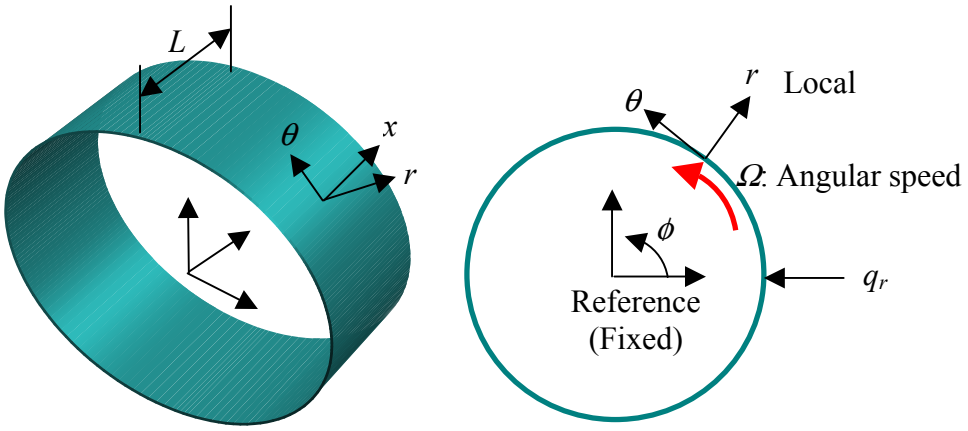

Figure 1: Model of tire treadband: a circular cylindrical shell with simply supported boundary conditions at the treadband edges.

2. Tire Treadband Model

Fig. 1 shows a cylindrical shell model of a tire treadband: the shell is assumed to rotate about a fixed axis coincident with the origin of reference coordinate system. The local coordinate system attached to the treadband rotates with the treadband. The effects of inflation pressure and rotational stiffening were represented through resultant in-plane residual stresses. However, static deformation of the shell due to either inflation or rotation was neglected: the treadband was assumed to vibrate around its static, uninflated shape. When shear deformation, rotary inertia and non-linear effects are neglected, a set of equations describing the three-dimensional motion of the shell can be derived in local coordinates [5]. Those equations can be transformed into the reference coordinate system by application of Reynolds' theorem: i.e.,

$$\frac{D}{Dt} = \frac{\partial}{\partial t} + \Omega \frac{\partial}{\partial \phi}, \tag{1}$$

where the left hand side represents the time derivative in local (Lagrangian) coordinates, the first term of the right hand side is the time derivative in global (Eulerian) coordinates, Ω is the angular rotational speed and ϕ is circumferential angle in the reference frame. After applying Eq. (1), the governing equations can be expressed as

$$L_x(u_x,u_\phi,u_r)+\lambda\frac{Du_x}{Dt}+\rho h\frac{D^2u_x}{Dt^2}=q_x(x,\phi,r) \tag{2-1}$$

$$L_\phi(u_x,u_\phi,u_r)+\lambda\frac{Du_\phi}{Dt}+\rho h\left(\frac{D^2u_\phi}{Dt^2}+2\Omega\frac{Du_r}{Dt}-\Omega^2u_\phi\right)=q_\phi(x,\phi,r) \tag{2-2}$$

$$L_r(u_x,u_\phi,u_r)+\lambda\frac{Du_r}{Dt}+\rho h\left(\frac{D^2u_r}{Dt^2}-2\Omega\frac{Du_\phi}{Dt}-\Omega^2u_r\right)=q_r(x,\phi,r) \tag{2-3}$$

$$L_x(u_x,u_\phi,u_r)=-\frac{\partial N_{xx}}{\partial x}-\frac{1}{a}\frac{\partial N_{\phi x}}{\partial\phi} \tag{2-4}$$

$$L_\phi(u_x,u_\phi,u_r)=-\frac{\partial N_{x\phi}}{\partial x}-\frac{\partial N_{\phi\phi}}{\partial\phi}-\frac{Q_{\phi r}}{a} \tag{2-5}$$

$$L_r(u_x,u_\phi,u_r)=-\frac{\partial Q_{xr}}{\partial x}-\frac{1}{a}\frac{\partial Q_{\phi r}}{\partial\phi}+\frac{N_{\phi\phi}}{a}-N^r_{xx}\frac{\partial^2u_r}{\partial x^2}-\frac{N^r_{\phi\phi}}{a^2}\frac{\partial^2u_r}{\partial\phi^2}, \tag{2-6}$$

where u is the displacement in the direction indicated by the subscript, N and Q are resultant normal and shear forces, respectively, the superscript r denotes residual force, and q is the external force applied in the direction indicated by the subscript. In addition, ρ is the density of the treadband, h is its thickness, λ is the damping constant, and a is the tire radius. The circumferential resultant normal force, $N_{\phi\phi}{}^r$, is related to inflation pressure and rotation speed by

$$N^r_{\phi\phi}=ap+\rho ha^2\Omega^2 \tag{3}$$

where p is the inflation pressure. The linear operators, L_i ($i = x,\phi, r$), are associated with the system's stiffness and thus Eq. (3) indicates how inflation pressure and rotation affect the treadband's stiffness. When the two terms on the right hand side of Eq. (3) are compared, it can be concluded that the stiffening effects associated with rotation may be ignored for a typical car tire running at normal speeds. That result will be demonstrated later in the paper.

3. Wave Solutions

As a first step towards obtaining analytical solutions to Eqs. (2-1) to (2-3), simple support conditions were considered to apply constraints in the radial and circumferential, but not the x-direction, at the treadband edges. In that case, a set of displacements satisfying those boundary conditions, i.e., sinusoidal or cosinusoidal functions in the x-direction, as appropriate, can be identified. That set must also be periodic in the circumferential direction. Based upon these various conditions, the set of displacements were assumed to have the wave-like form

$$u_{xmn}(x,\phi) = \sum_{m=1}^{\infty}\sum_{n=-\infty}^{\infty} A_{mn}\cos\left(\frac{m\pi x}{L}\right)\exp\left(i\omega_{mn}t - in\phi\right) \tag{4-1}$$

$$u_{\phi mn}(x,\phi) = \sum_{m=1}^{\infty}\sum_{n=-\infty}^{\infty} B_{mn} i\sin\left(\frac{m\pi x}{L}\right)\exp\left(i\omega_{mn}t - in\phi\right) \tag{4-2}$$

$$u_{rmn}(x,\phi) = \sum_{m=1}^{\infty}\sum_{n=-\infty}^{\infty} C_{mn}\sin\left(\frac{m\pi x}{L}\right)\exp\left(i\omega_{mn}t - in\phi\right) \tag{4-3}$$

where the coefficients A, B and C are assumed to be real. By substituting Eqs. (4) into Eqs. (2), and setting the input force and damping to zero, a matrix equation similar to an eigenvalue problem is obtained: i.e.,

$$\begin{bmatrix} k_{11mn} - \rho h\varpi_{mn}^{\ 2} & k_{12mn} & k_{13mn} \\ k_{12mn} & k_{22mn} - \rho h(\varpi_{mn}^{\ 2} + \Omega^2) & k_{23mn} - 2\rho h\Omega\varpi_{mn} \\ k_{13mn} & k_{23mn} - 2\rho h\Omega\varpi_{mn} & k_{33mn} - \rho h(\varpi_{mn}^{\ 2} + \Omega^2) \end{bmatrix}\begin{bmatrix} A_{mn} \\ B_{mn} \\ C_{mn} \end{bmatrix} = \begin{bmatrix} 0 \\ 0 \\ 0 \end{bmatrix}, \tag{5-1}$$

where

$$\varpi_{mn} = \omega_{mn} - n\Omega. \tag{5-2}$$

In Eq. (5-1), the stiffness terms, k_{ij} (i,j=1,2,3), are associated with the linear operators in Eqs. (2). Further, in Eq. (5-2) the left hand side is the natural frequency in local coordinates while the first term on the right hand side is the natural frequency in reference coordinates. For future reference, Eq. (5-2) will be denoted the "kinematics relation". The characteristic equation obtained from Eq. (5-1) is sixth order: i.e., there are six natural frequencies associated with each (m,n) wave mode. However, the negative-going wave mode (m,-n) has the same natural frequency as the positive-going (m,n) wave mode. Thus, when a local natural frequency is defined to be positive, the sign convention used in the assumed displacements means that a positive n denotes a positive-going wave and a negative n a negative-going wave. It can thus be concluded that there are only three distinct natural frequencies associated with each (m,n) wave mode. Each of those frequencies is associated with a particular wave type: i.e., flexural, longitudinal, or shear.

The natural frequencies can be found from the characteristic equation derived from Eq. (5-1) as can the associated modal vectors. The forced response can then be expressed as a superposition of wave modes: i.e.,

$$u_x(x,\phi,t) = \sum_{m=1}^{\infty}\sum_{n=-\infty}^{\infty}\sum_{l=1}^{3} A_{mnl}\cos\left(\frac{m\pi x}{L}\right)\exp\left(-in\phi\right)\eta_{mnl}(t) \tag{6-1}$$

$$u_\phi(x,\phi,t) = \sum_{m=1}^{\infty}\sum_{n=-\infty}^{\infty}\sum_{l=1}^{3} iB_{mnl}\sin\left(\frac{m\pi x}{L}\right)\exp\left(-in\phi\right)\eta_{mnl}(t) \tag{6-2}$$

$$u_r(x,\phi,t) = \sum_{m=1}^{\infty}\sum_{n=-\infty}^{\infty}\sum_{l=1}^{3} C_{mnl}\sin\left(\frac{m\pi x}{L}\right)\exp\left(-in\phi\right)\eta_{mnl}(t), \tag{6-3}$$

where the l index represents the three natural frequencies for each wave mode. The modal weighting function, η_k(t), can be calculated by substituting Eqs. (6) into Eqs. (2) and then applying Eq. (5) with forcing terms included. The result is

$$\ddot{\eta}_k + \left(\frac{\lambda}{\rho h} + i2\Omega(n+2\gamma_k) \right) \dot{\eta}_k + \left(\omega_k^2 - 2\Omega\omega_k(n+2\gamma_k) - in\Omega\frac{\lambda}{\rho h} \right) \eta_k = \frac{Q_k}{\rho h N_k}, \tag{7-1}$$

where

$$N_k = \pi L\left(A_k^2 + B_k^2 + C_k^2\right) \tag{7-2}$$

$$\gamma_k = \frac{B_k C_k}{A_k^2 + B_k^2 + C_k^2} \tag{7-3}$$

$$Q_k = \int_0^{2\pi}\int_0^L \left[q_x A_k \cos\left(\frac{m\pi x}{L}\right) + q_\phi B_k i \sin\left(\frac{m\pi x}{L}\right) + q_r C_k \sin\left(\frac{m\pi x}{L}\right) \right] e^{in\phi} dx d\phi. \tag{7-4}$$

Eq. (7-1) may then be solved for η_k(t).

Table 1: Material parameters for tire treadband.

Young's Modulus	$E = 4.8\times10^8$ N/m^2
Density	$\rho = 1200$ kg/m^3
Thickness	$h = 0.008$ m
Poisson's ratio	$\nu = 0.45$
Radius	$a = 0.32$ m
Width	$L = 0.16$ m
Damping ratio	$\zeta = 0.05$
Inflation pressure	$p = 206910$ Pa ($p = 30$ psi)
Sidewall tension	$N_x^r = 2\times10^4$ N/m

4. Results and Discussion

The material parameters used here are listed in Table 1: they were adapted from the literature, were based on physical reasoning, or were obtained by direct measurement.

Fig. 2 shows the dispersion relations obtained by solving the system characteristic equation. Note that k_ϕ in the x-axis of the figures is the circumferential wave number which is related to the circumferential mode number, n, by $k_\phi = n/a$. Thus, the dispersion relations are defined at a set of discrete points. Here each trajectory of the dispersion relation is associated with a cross-sectional mode index: i.e., m = 1, etc. in Fig. 2(a). For each combination of circumferential and cross-sectional mode numbers, there are three natural frequencies associated primarily with flexural, shear, and longitudinal motions in order of increasing frequency [2]. The static dispersion relations are plotted in Fig. 2(a). In Fig. 2(b), the local natural frequencies are plotted when the rotation speed was set to the artificially large value of Ω= 500 rad/s to amplify the effects of rotation: a more typical range is from Ω= 0 to Ω= 100 rad/s. By comparison with Fig. 2(a), two phenomena can be observed. First, it can be seen that the wave speed is increased by rotational

stiffening (i.e., the slope of the modal trajectories is increased.). Secondly, on close examination, it can be seen that the dispersion curves are asymmetrical with respect to the zero wave number axis: this is the so-called "bifurcation" effect. This asymmetry means that the speeds of waves propagating in opposite directions with the same wavelengths are different even when observed in local coordinates. However, the present results indicate that this effect is negligible under normal circumstance. Results in local coordinates for a more typical speed, $\Omega = 100$ rad/s, are plotted in Fig. 2(c). By comparison with the $\Omega = 0$ results, it can be seen that the stiffening due to rotation is not very significant in this case, as explained earlier in connection with Eq. (3). Finally, the dispersion relations in the reference frame are plotted in Fig. 2(d), also for $\Omega = 100$ rad/s. Note that the latter results were obtained from those of Fig. 2(c) after applying the kinematics relation, Eq. (5-2). In Fig. 2(d), the asymmetry resulting from the kinematic effect of tire rotation is very clear in contrast with the bifurcation effect in the local coordinates (Fig. 2(c)).

For the purpose of validating the modeling and solution procedures, the stationary model ($\Omega = 0$) was reproduced using a FE model [2]. The corresponding wave number-transformed forced solutions (presented as radial velocity magnitude) for a radial point force on the treadband centerline calculated using FE and analytical procedures are plotted in Fig. 3. The two results are identical for practical purposes.

The spatial distribution of the centerline radial velocity for a radial point force applied on the centerline and fixed with respect to the reference frame (simulating a contact patch excitation) is plotted in the reference frame in Fig. 4(a), and the corresponding circumferential wave number transformed results are shown in Fig. 4(b). Note that zero deg. in Fig. 4(a) indicates the drive point. One interesting aspect of these results is that standing wave patterns appear even under rotation. The standing waves are made possible by damping, since the latter causes the dispersion trajectories to have a finite width, thus making it possible for there to be components propagating in opposite directions with the same wavelength at the same frequency. A comparison of the responses in the positive and negative ϕ regions of Fig. 4(a) shows that the standing wave pattern is more obvious in the region $\phi < 0$: i.e., upstream of the drive point. It can also be seen that there are no even modes in the results of Fig. 4(b) (compare with Fig. 2(d)) since the point force was applied at the center of treadband. Also note that the trajectories in Fig. 4(b) are continuous (not discrete as in Fig. 2) because of the effect of damping. Finally, note that the asymmetry of the trajectory slopes in Fig. 4(b) indicates that waves travel more quickly downstream ($k_\phi > 0$) as expected. Since both rotational stiffness and bifurcation effects are essentially negligible, it is possible to map the static forced response (Fig. 3(b)) onto the rotation response by using Eq. (5-2).

5. Conclusion

In the work described here, the treadband of a tire was modeled as a rotating circular cylindrical shell in order to identify the effects of rotation. A wave-based solution procedure was applied to obtain analytical solutions for both free and forced vibration cases. This procedure has been verified by comparison with FE simulations. It was shown that rotation has two principal effects: stiffening of the treadband and "tilting" of the dispersion curves. It was found, however, that the rotational stiffening effect was not significant compared with the effect of inflation pressure at typical rotational speeds. In contrast, the kinematic tilting effect was found to be significant. Thus, it was concluded that a linear function, Eq. (5-2), could be used to adjust the static dispersion curve which could then be used to analyze the potential of a rotating tire to radiate sound.

References

1. J. S. Bolton and Y.-J. Kim, Wave number domain representation of tire vibration, *Proc. of INTER-NOISE 2000*, **1**, 184-190, 2000.
2. Y.-J. Kim and J. S. Bolton, Modeling tire treadband vibration, *Proc. of INTER-NOISE 2001*, 2001.
3. S. C. Huang and W. Soedel, Effects of Coriolis acceleration on the forced vibration of rotating cylindrical shells, *Journal of Applied Mechanics*, **55**, 231-233, 1988.
4. E. Vinesse and H. Nicollet, Surface waves on the rotating tyre: An application of functional analysis, *Journal of Sound and Vibration*, **126**(1), 85-96, 1988.
5. W. Soedel, *Vibrations of Shells and Plates*, 2nd ed., Marcel Dekker Inc., 1993.

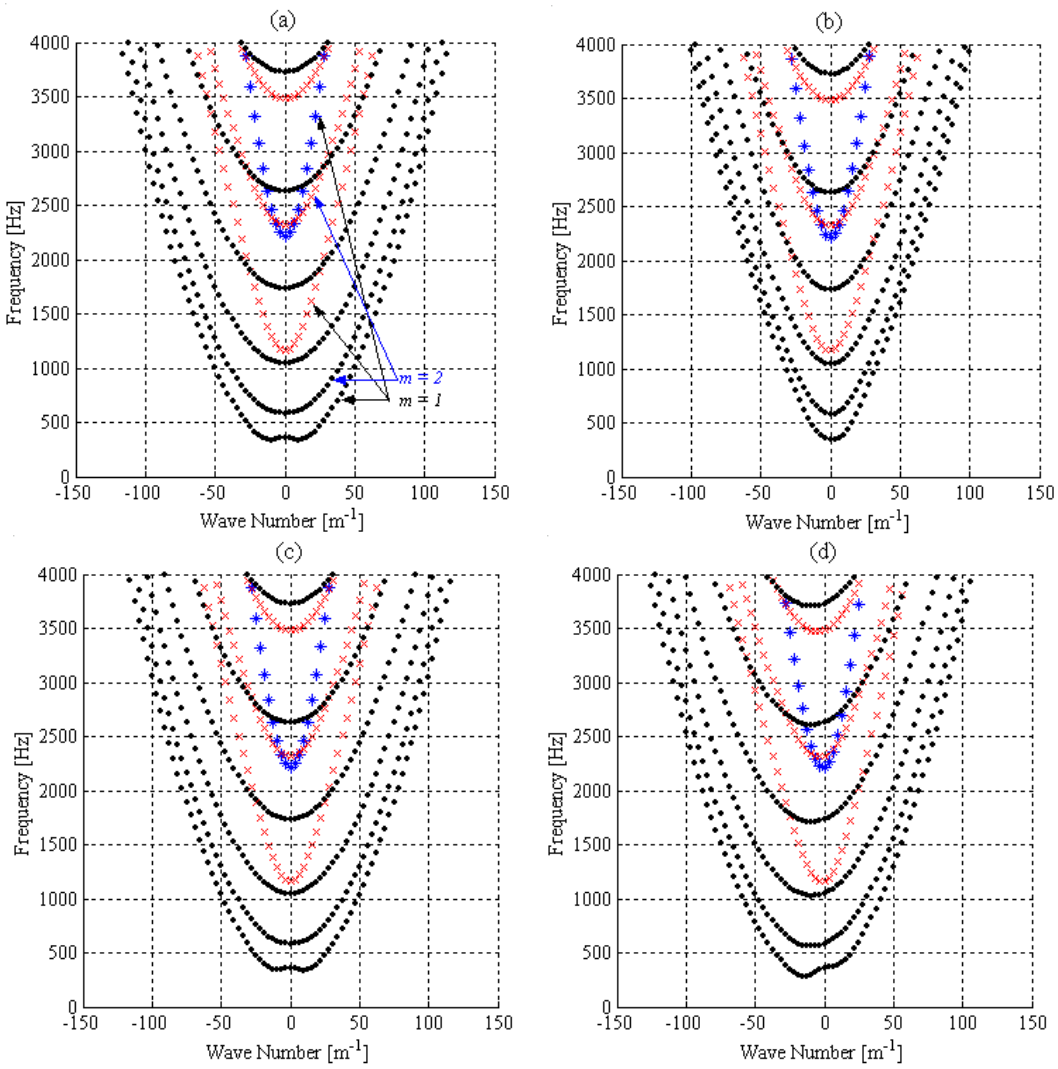

Figure 2: Dispersion relations derived from characteristic equation: • - flexural wave, × - shear wave, and * - longitudinal wave: (a) $\Omega = 0$, (b) natural frequencies in local coordinates when Ω = 500 rad/s, (c) natural frequencies in local coordinates when Ω = 100 rad/s and (d) natural frequencies in reference coordinates when Ω = 100 rad/s.

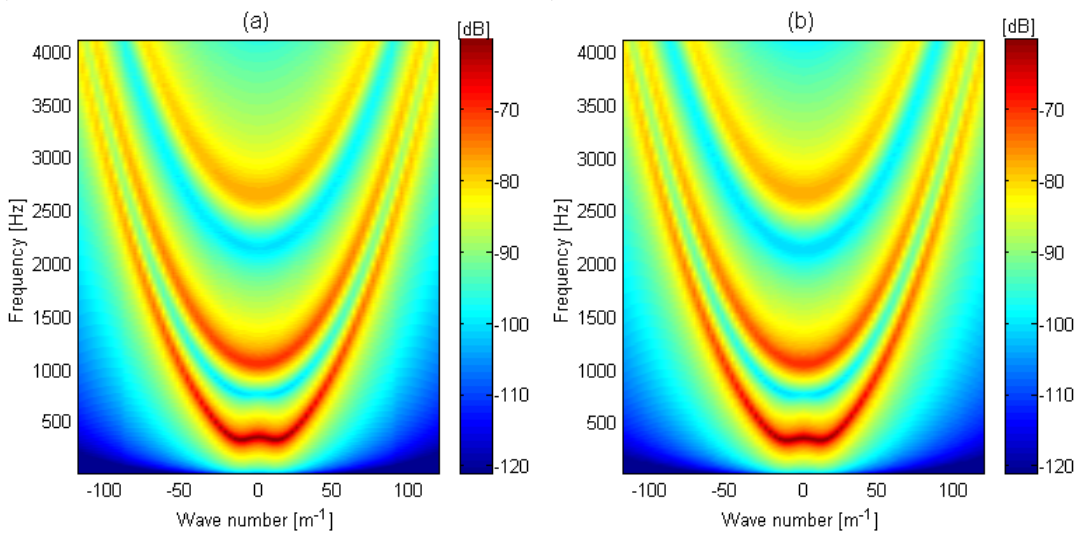

Figure 3: Comparison of analytical forced response with FE simulation when $\Omega = 0$: (a) FE simulation and (b) analytical solution.

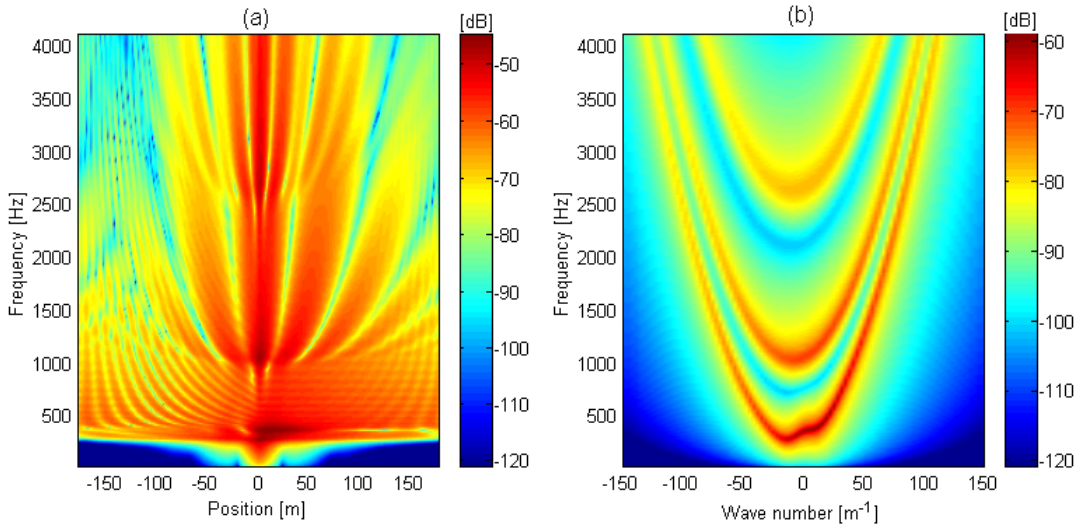

Figure 4: Forced response when $\Omega = 100$ rad/s: (a) amplitude of vibration at treadband center and (b) dispersion relation obtained by circumferential wave number transform.